photonics

MDPI

Article

Enhanced Emission Properties of Dysprosium Ions Doped Lead Borophosphate Zinc Barium Glasses for White Light Luminescent Applications

Valluri Ravi Kumar [1], S. V. B. Subrahmanyeswararao [2], K. Kiran Kumar [3], B. Venkata Manikanta [2], K. Swathi [3], L. Mounica [3], M. Nagarjuna [4], V. Sujatha [5], L. Vijayalakshmi [6,*] and Jiseok Lim [6,*]

1 Department of Physics, Ramachandra College of Engineering, Eluru 534007, Andhra Pradesh, India; ravikumar89@rcee.ac.in
2 Department of Mathematics, Ramachandra College of Engineering, Eluru 534007, Andhra Pradesh, India
3 Department of Chemistry, Kakaraparti Bhavanarayana College, Vijayawada 520001, Andhra Pradesh, India
4 Department of Physics, Dhanekula Institute of Engineering & Technology, Vijayawada 521139, Andhra Pradesh, India
5 Department of Physics, DVR & Dr HS MIC College of Technology, Kanchikacherla 521180, Andhra Pradesh, India
6 Department of Mechanical Engineering, Yeungnam University, Gyeongsan-si 38541, Republic of Korea
* Correspondence: lvl.phy@gmail.com (L.V.); jlim@yu.ac.kr (J.L.)

Abstract

Lead borophosphate zinc barium glass systems doped with different concentrations of Dy_2O_3 (0.5–2.0 mol%) were fabricated using the traditional melt-quenching method. The non-crystalline nature of the synthesized glass samples was verified through X-ray diffraction (XRD) analysis, which exhibited the characteristic absence of sharp diffraction peaks. Morphological, structural, and vibrational properties were analyzed using scanning electron microscopy (SEM) and Fourier infrared transmission (FTIR) spectroscopy. Optical absorption, emission, and decay lifetime observations were recorded to evaluate the luminescence behavior of Dy^{3+} ions. Judd–Ofelt parameters (Ω_2, Ω_4, and Ω_6) were evaluated from the optical absorption spectra of all the prepared glass samples. The emission spectra revealed three dominant transitions in the visible region corresponding to the $^4F_{9/2} \longrightarrow {}^6H_{15/2}$ (blue ~ 484 nm), $^4F_{9/2} \longrightarrow {}^6H_{13/2}$ (yellow ~ 574 nm), and $^4F_{9/2} \longrightarrow {}^6H_{11/2}$ (~663 nm) transitions. Radiative characteristics, including radiative transition probability (A_R), radiative lifetime (τ_R), and branching ratio (β_R), were calculated from the emission spectra. Among the investigated compositions, the host glass embedded with 1.0 mol% Dy_2O_3 demonstrated the maximum emission intensity was observed along with superior quantum efficiency (η = 91.68%). The chromaticity coordinates for this composition (x = 0.33, y = 0.41) are positioned close to the white-light region in the CIE 1931 chromaticity diagram. These findings suggest that incorporating 1.0 mol% of Dy_2O_3 yields the highest luminescence efficiency, making the present glass system a promising candidate for white-light-emitting and photonic device applications.

Keywords: PbO-B_2O_3-P_2O_5-ZnO-BaO glasses; Dy^{3+} ions; J-O parameters; PL efficiency; white-light luminescent applications

Check for updates

Received: 29 January 2026
Revised: 21 February 2026
Accepted: 27 February 2026
Published: 28 February 2026

Copyright: © 2026 by the authors. Licensee MDPI, Basel, Switzerland. This article is an open access article distributed under the terms and conditions of the Creative Commons Attribution (CC BY) license.

1. Introduction

Glasses incorporating dysprosium oxide (Dy_2O_3) are commonly utilized as white-light-emitting materials due to their distinctive emission transitions, which are well recognized.

Especially, these glasses exhibit blue and yellow emission transitions, viz., $^4F_{9/2} \rightarrow {}^6H_{15/2}$ (electronic dipole) and $^4F_{9/2} \rightarrow {}^6H_{13/2}$ (magnetic dipole). The emission intensity ratio (Y/B) is different for different materials and significantly influences white-light generation. Moreover, Dy^{3+} ions exhibit emission bands at about 3.02 µm ($^6H_{13/2} \rightarrow {}^6H_{15/2}$) and 1.34 µm ($^6H_{11/2} \rightarrow {}^6H_{13/2}$) for optical fiber amplifier applications [1–6].

Dysprosium (Dy^{3+})-doped glasses have garnered significant attention due to their versatile luminescent properties arising from characteristic $^4F_{9/2} \rightarrow {}^6H_{15/2}$ (blue, ~480 nm) and $^4F_{9/2} \rightarrow {}^6H_{13/2}$ (yellow, ~570 nm) transitions, enabling white-light emission when these bands are balanced appropriately. This makes Dy^{3+}-activated materials promising for solid-state lighting and display technologies. However, their utility spans beyond this, into fields like optical amplifiers, sensors, and radiation shielding, depending on the glass host and co-dopants used [7].

Compared to other rare earth ions such as Er^{3+}, Nd^{3+}, and Yb^{3+}, which are predominantly used in optical amplifiers and telecommunication devices, and Eu^{3+} and Tb^{3+} ions, which exhibit red and green emissions suitable for display technologies, Dy^{3+} ions doped glasses are relatively less explored in commercial applications. However, Dy^{3+} ions offer distinctive advantages through their simultaneous emission (blue) $^4F_{9/2} \rightarrow {}^6H_{15/2}$ and (yellow) $^4F_{9/2} \rightarrow {}^6H_{13/2,}$ respectively, enabling near-white-light generation from a single activator. Furthermore, Dy^{3+}-activated glass possesses superior chemical stability, lower fabrication cost, and easier processability compared to conventional YAG: Ce phosphors. The strong sensitivity of Dy^{3+} emissions to local field symmetry and temperature also makes these materials promising candidates for optical thermometry and pressure sensing applications.

For these reasons, the current Dy^{3+} ions doped glass system is not merely an extension of known applications but an attempt to converge multiple functionalities of white-light generation, shielding, and optical sensing into a single platform. While other rare-earth systems may outperform Dy^{3+} ions in specialized roles, this ion offers a unique combination of optical characteristics and structural adaptability, especially in low-phonon glass hosts like PBPZBa. This broader perspective situates the study in the context of multifunctional rare-earth-doped materials, and the manuscript can benefit from including such a review to justify the material choice.

The luminescent behavior of rare earth Dy^{3+} ions doped lead borophosphate zinc barium glasses in the UV, visible, and NIR spectral regions. These glass materials are particularly applicable for applications in the white-light-emitting diodes, optical amplifiers, fiber optics, radiation shielding, and optical sensing. The presence of P_2O_5 and B_2O_3 promotes the formation of linkages B-O-P between PO_4 and BO_4 structural units. Such linkages contribute to a more interconnected glass network [8,9]. Incorporating lead oxide (Pb_3O_4) enhances the physical attributes like density and refractive index, and improves resistance to devitrification, as well as moisture degradation. Incorporating BaO and ZnO is essential for optimizing luminescence performance, structural robustness, and strong resistance to thermal degradation, which makes them promising candidates for advanced optical, photonic, and radiation shielding applications as mentioned [10,11].

In recent years, significant efforts have been devoted to understanding the incorporation mechanism and photoluminescence behavior of Dy^{3+} ions in various amorphous glass matrices, particularly borophosphate, borosilicate, tellurite, and lead-phosphate systems. Previous studies have demonstrated that the local structural environment, site symmetry, and covalency around Dy^{3+} ions strongly influence the intensity ratio of the $^4F_{9/2} \rightarrow {}^6H_{15/2}$ (blue) and $^4F_{9/2} \rightarrow {}^6H_{13/2}$ (yellow) transitions, which governs white-light generation. Judd–Ofelt analysis has been widely employed to evaluate the radiative properties and to correlate Ω_2 values with structural asymmetry in rare-earth-doped glasses. Furthermore,

concentration quenching, cross-relaxation, and energy migration processes have been identified as key factors limiting emission efficiency at higher dopant levels. In multicomponent glass systems, network formers such as B_2O_3 and P_2O_5 and modifiers like PbO, ZnO, and BaO play a crucial role in tailoring the phonon energy, non-bridging oxygen content, and local crystal field strength, thereby directly affecting Dy^{3+} luminescence performance. Therefore, a systematic investigation of Dy^{3+} incorporation in Pb–B–P–Zn–Ba-based amorphous matrices is essential for optimizing white-light emission and enhancing photonic device applicability.

The present study investigates the impact of varying Dy^{3+} ion concentrations (0.5, 1.0, 1.5, and 2.0 mol%) in PbO-B_2O_3-P_2O_5-ZnO-BaO glasses on white-light luminescence. Among these, Dy10 glass exhibits the maximum luminescence intensity compared to other concentrations of Dy^{3+}-doped glasses. This enhanced luminescence is attributed to lower non-radiative losses in the glass matrix. To better understand, the structural morphological investigations were carried out through X-ray diffraction, SEM, and FTIR studies.

2. Experimental

The detailed glass sample composition in the present study is as follows:
$PBPZBaDy_5$: 10PbO-20B_2O_3-49.5 P_2O_5-10ZnO-10BaO-0.5 Dy_2O_3;
$PBPZBaDy_{10}$: 10PbO-20B_2O_3-49.0 P_2O_5-10ZnO-10BaO-1.0 Dy_2O_3;
$PBPZBaDy_{15}$: 10PbO-20B_2O_3- 48.5 P_2O_5-10ZnO-10BaO-1.5 Dy_2O_3;
$PBPZBaDy_{20}$: 10PbO-20B_2O_3-48.0 P_2O_5-10ZnO-10BaO-2.0 Dy_2O_3.

High-purity chemical reagents, including PbO, H_3BO_3, P_2O_5, ZnO, $BaCO_3$, and Dy_2O_3, were weighed with precision and uniformly blended with an agate mortar. The uniform powder mixture was melted in a silica crucible at 1350 °C for one hour using a PID-controlled furnace. After obtaining a homogeneous melt, the liquid was poured into a pre-heated brass mold and subjected to annealing at 450 °C to relieve residual internal stresses within the prepared samples. Synthesized glass samples exhibited an amorphous nature, which was verified through XRD analysis carried out using a Rigaku D/Max ULTIMA III diffractometer (Rigaku Corporation, Tokyo, Japan) utilizing CuKα radiation. The prepared glass samples were optically polished to dimensions of approximately 1.0 × 0.2 cm^2, and their densities were measured using Archimedes' principle with o-xylene employed as the liquid medium. Refractive index values were calculated using an Abbe refractometer with mono-bromonaphthalene as the contact medium, utilizing a sodium light source (589.3 nm wavelength). Optical absorption spectra of the fabricated samples were recorded at room temperature over the wavelength range 200–1800 nm using a UV-Vis-NIR spectrophotometer (JASCO Corporation, Tokyo, Japan). Emission spectra for all the glasses were obtained at room temperature using a (Lumina) Thermo Scientific luminescence spectrophotometer (Thermo Fisher Scientific, Waltham, MA, USA) operating within a wavelength range of 200 to 900 nm. The lifetime decay measurements are performed following methodologies outlined in previous studies [12,13].

In the present glass compositions, Dy_2O_3 was incorporated by partially substituting P_2O_5 while maintaining the total molar percentage at 100 mol%. P_2O_5 acts as a primary glass former in the borophosphate network; therefore, its gradual reduction compensates for the introduction of Dy^{3+} ions without significantly disturbing the overall glass-forming ability. The substitution strategy ensures compositional consistency across all samples and enables a systematic investigation of the influence of Dy^{3+} concentration on structural and luminescence properties. The incorporation of Dy^{3+} ions in place of P_2O_5 is expected to modify the local network connectivity by generating non-bridging oxygens (NBOs) and altering the P–O–P and B–O–P linkages, which in turn affects the optical and radiative characteristics of the prepared glasses.

3. Results and Discussion

Physical properties of the prepared glass samples with different Dy^{3+} ion concentrations were evaluated using established formulas [14,15], measured molecular weight (M), density (ρ), refractive index (n_d), and the experimentally determined parameters. The related physical properties were summarized in Table 1.

Table 1. Physical parameters of Dy^{3+} ions doped PbO-B_2O_3-P_2O_5-ZnO-BaO glasses.

Glass Sample	Avg. Mo. Wt. M	Density d (g/cm^3)	Dy^{3+} Ion Conc. N_i (10^{19}/cm^3)	Inter Ionic Distance of Dy^{3+} Ions R_i (nm)	Refractive Index, n_d	Optical Band Gap (E_o)
PBPZBaDy5	248.37	3.75	4.55	2.80	1.613	3.78
PBPZBaDy10	248.82	3.82	9.15	2.21	1.635	3.73
PBPZBaDy15	249.27	3.81	1.38	1.93	1.619	3.85
PBPZBaDy20	249.71	3.80	1.85	1.75	1.626	3.88

The density of each glass sample was determined based on Archimedes principle using o-xylene as the immersing liquid, following the relationship [13,16]:

$$\rho(\mathrm{gm/cm^3}) = \left[\frac{\mathrm{Wa}}{\mathrm{Wa} - \mathrm{Wb}}\right] \times \rho_b \quad (1)$$

the weight of the glass sample in air is denoted by W_a, while W_b represents the weight of the glass sample when submerged in o-xylene. The density of o-xylene is given as $\rho_b = 0.86$ g/cm^3. The molar volume (V_m) of the glass samples was determined using the following formula:

$$V_m = MT/\rho \quad (2)$$

Here ρ represents the density of the samples, and MT denotes the total molecular weight of the multi-component of the glass system, determined using the following relation:

$$MT = XPbO + XB_2O_3 + XP_2O_5 + XZnO + XBaO \quad (3)$$

where X is molar fraction of the chemical component.

The refractive index (n_d) of the samples was determined directly using an Abbe refractometer.

Figure 1 illustrates variation in density (ρ) and refractive index (n_d) as a function of Dy^{3+} ion concentration. The results indicate that increasing Dy^{3+} from 0.5 to 1.0 mol% enhances both density and refractive index. At lower Dy_2O_3 concentrations (0.5–1.0 mol%), the high field strength and relatively large atomic mass of Dy^{3+} enhance Dy–O bond strength and improve local structural compactness without significantly disrupting the glass network. The FTIR spectra support this interpretation. For the 1.0 mol% sample, the bands corresponding to asymmetric P–O–P and B–O–P linkages (around ~1080–910 cm^{-1}) show relative strengthening, indicating improved cross-linking between BO_4 and PO_4 units and reduced structural disorder. This enhanced network connectivity and compact packing explain the observed increase in density (3.75 → 3.82 g/cm^3) and refractive index (1.613 → 1.635).

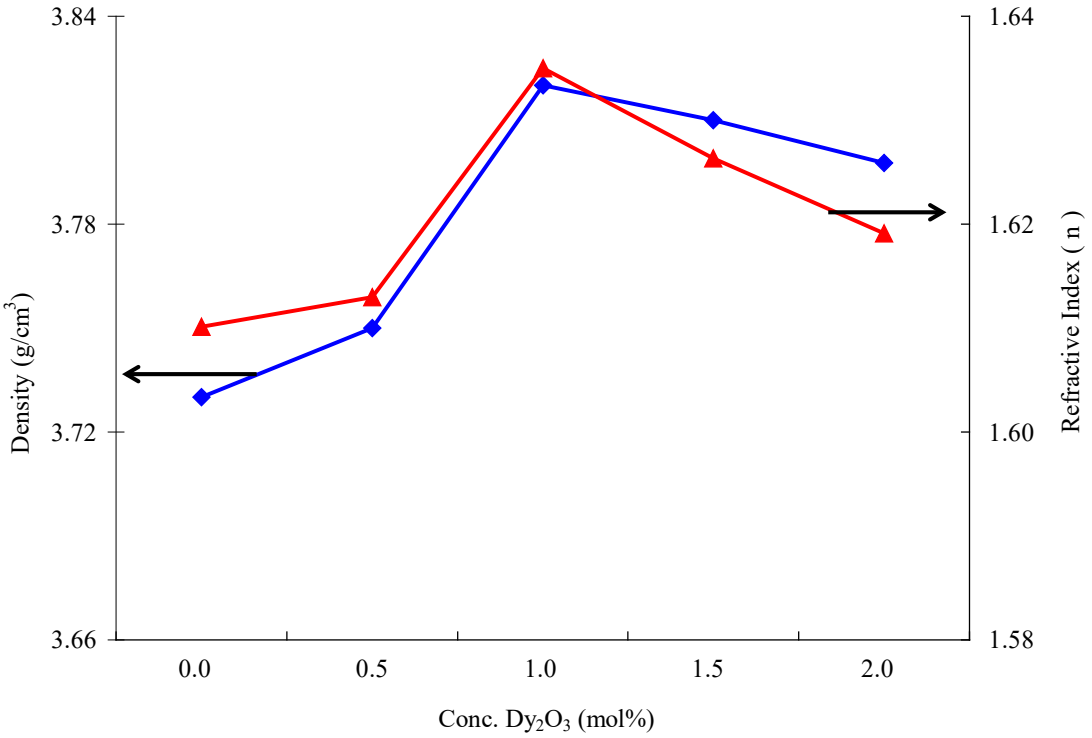


Figure 1. Variation in density (g/cm^3) and refractive index (n_d) of Dy^{3+} ions doped PbO-B_2O_3-P_2O_5-ZnO-BaO glasses.

However, beyond 1.0 mol% Dy_2O_3, excessive incorporation of Dy^{3+} leads to the formation of additional non-bridging oxygens (NBOs) and partial disruption of P–O–P/B–O–P linkages, as indicated by the relative enhancement of bands associated with PO_2^- and BO_3 units in the FTIR spectra. Furthermore, possible Dy^{3+}-Dy^{3+} clustering at higher concentrations reduces network connectivity and structural compactness. This increased depolymerization explains the slight decrease in density and refractive index for 1.5 and 2.0 mol% samples. Thus, the non-linear trend reflects an initial network strengthening effect followed by depolymerization and ion clustering at higher Dy^{3+} content.

Figure 2 presents the X-ray diffractogram pattern for all the glass samples, confirming their amorphous structure within the glasses. Figure 3 shows the SEM image of $PBPZBaDy_{10}$ glass, revealing microscale surface features. These grain formations likely originated during the melting and annealing stages.

Figure 4 shows the FTIR spectra of $PBPZBaDy_{10}$ glass, which exhibits distinct vibrational bands corresponding to different structural units present in the borophosphate glass network. The bands observed at ~1280 cm^{-1} and 1240 cm^{-1} are associated with trigonal BO_3 and P=O bonds of PO_2^- stretching vibrations, respectively. These high-frequency bands arise from strong B-O and P=O bonds present in the network. The peak around 1080 cm^{-1} corresponds to the symmetric stretching vibrations of tetrahedral BO_4^- and PO_4^{3-} units. Another band near 910 cm^{-1} is assigned to asymmetric stretching vibrations of bridging P–O–P linkages, confirming the formation of a connected phosphate network. Additional bands at 780 cm^{-1} and 690 cm^{-1} indicate symmetric P–O–P and B–O–B band vibrations, which further support the presence of a mixed borophosphate structural framework. The low-frequency band around 500 cm^{-1} is attributed to Pb-O and Zn-O vibrations, indicating the participation of PbO_4 and ZnO_4 structural units acting as network modifiers. All the assigned bands are tabulated in Table 2. Notably, the asymmetric vibration bands of the highest intensity and slightly broadened in 1.0 mol% of Dy^{3+}-doped glasses suggest increased network disruption [17–21].

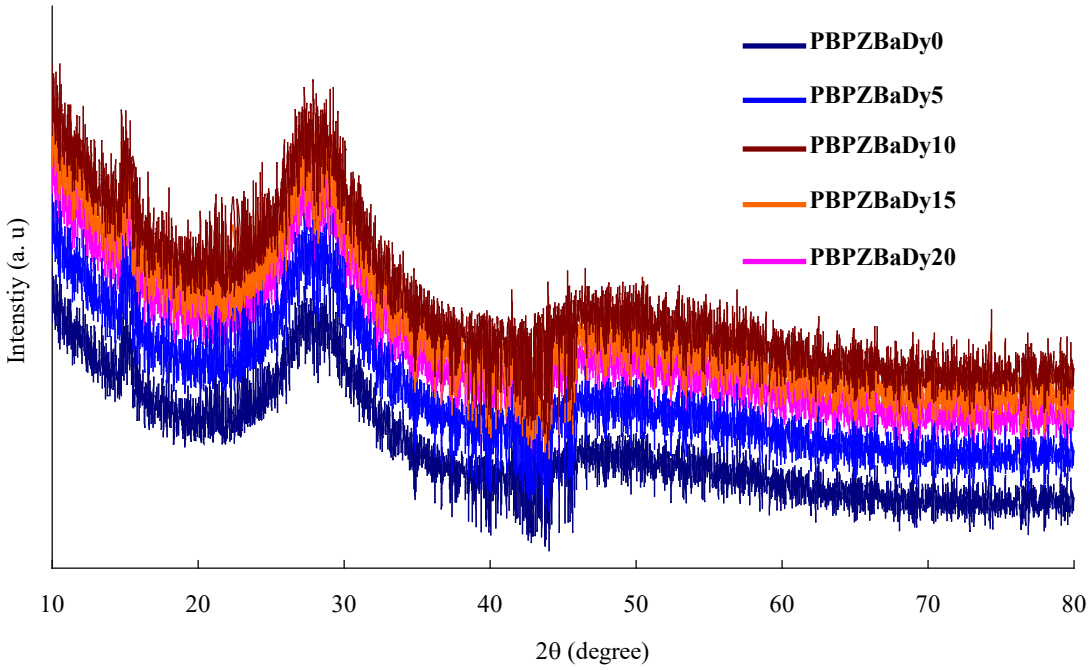


Figure 2. XRD patterns for Dy^{3+} ions doped PbO-B_2O_3-P_2O_5-ZnO-BaO glasses.

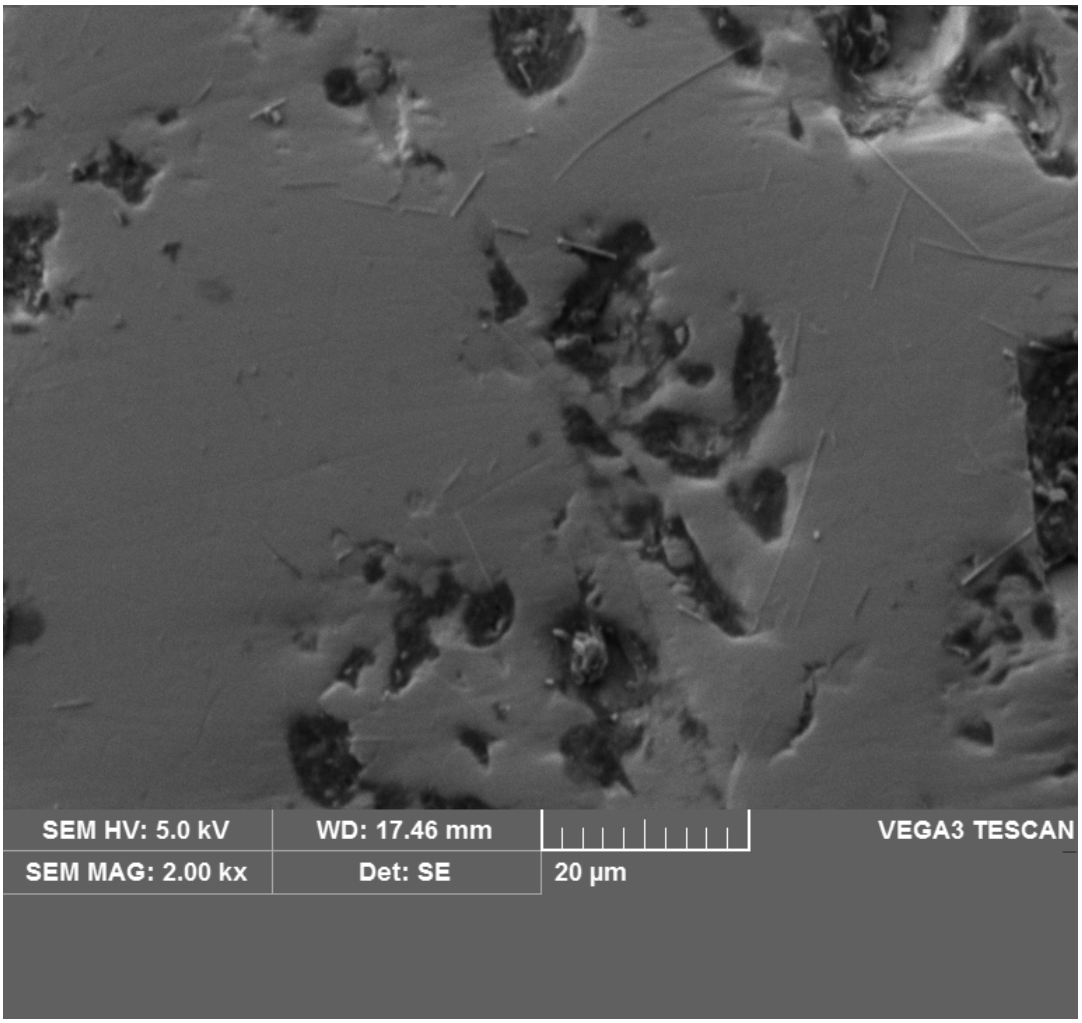


Figure 3. SEM photograph of PBPZBaDy10 glass.

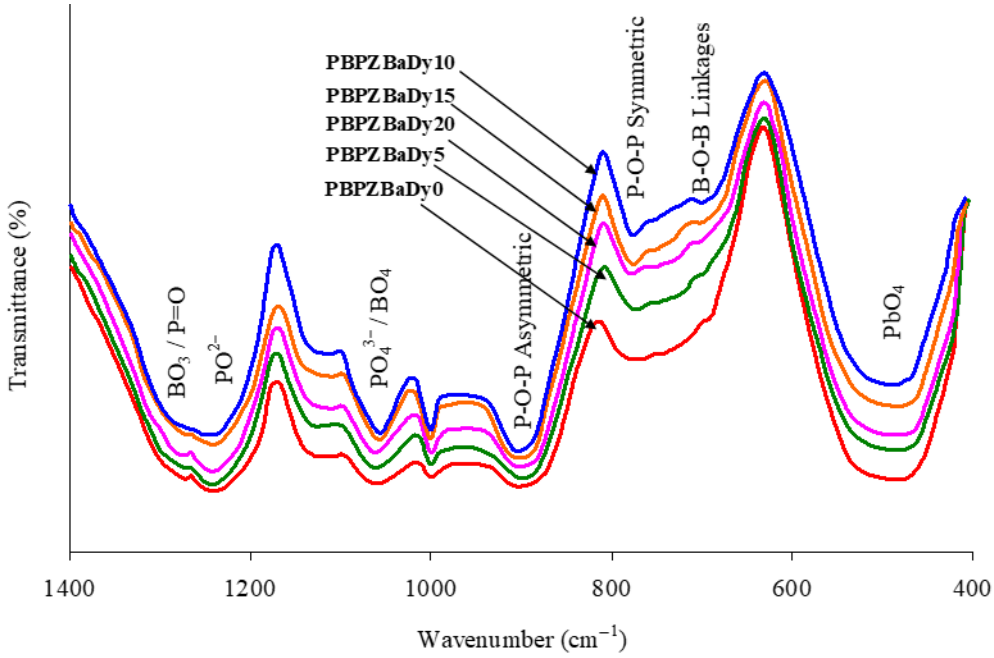


Figure 4. FT-IR spectra for Dy^{3+} ions doped PbO-B_2O_3-P_2O_5-ZnO-BaO glasses.

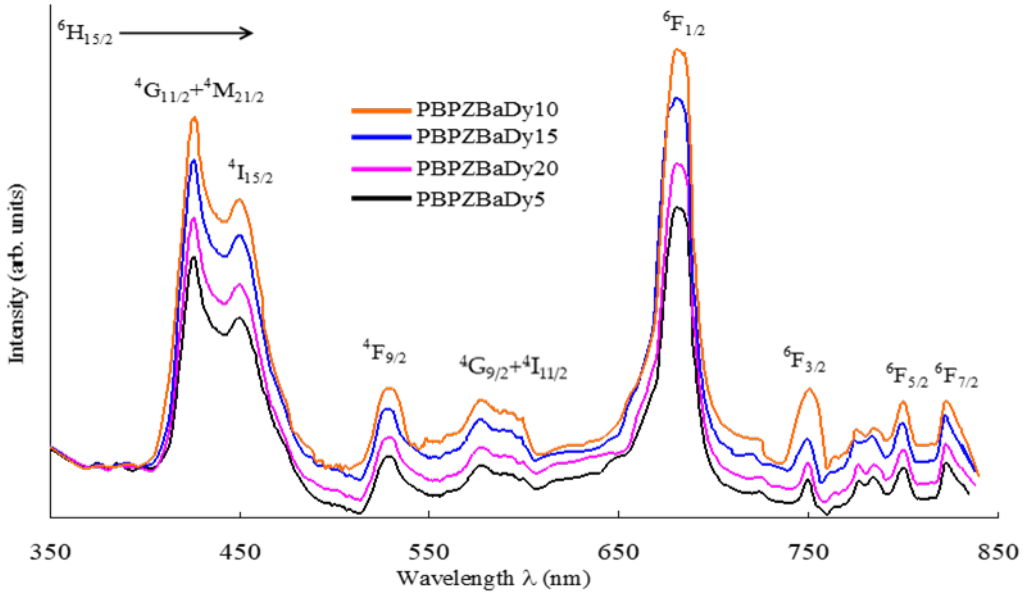
Table 2. Characteristic FTIR vibrational bands and their assignments for structural units in borophosphate glass systems.

Observed Region (cm^{-1})	Assignment
~1280–1240	BO_3/P=O and PO^{2-} Stretching
~1080	BO_4^- and PO_4^{3-} symmetric stretching
~910	Asymmetric P–O–P vibrations
~780	Symmetric P–O–P stretching
~690	B–O–B linkages
~500	PbO_4/ZnO_4 structural units

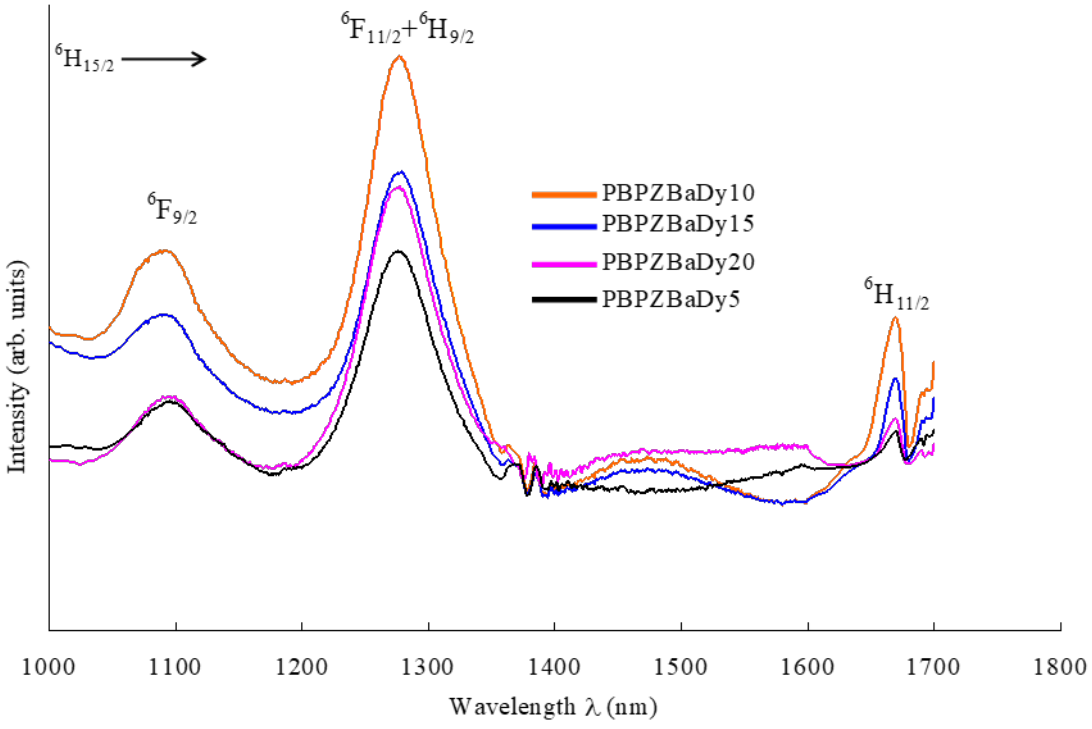
Figure 5a,b presents the absorption spectra of the labeled glass samples measured over a 200–2000 nm range. The spectra have exhibited the bands in the UV-vis-NIR region corresponding to 4f electron transitions of Dy^{3+} ions: $^6H_{15/2} \rightarrow {}^4G_{11/2}$ + $^4M_{21/2}$, $^4I_{15/2}$, $^4F_{9/2}$, $^4G_{9/2}$ + $^4I_{11/2}$, $^6F_{1/2, 3/2, 5/2, 7/2}$ (UV-vis region), and $^6F_{9/2,}$ $^6F_{11/2}$+$^6H_{9/2,}$ and $^6H_{11/2}$ (NIR region). Among these, the transitions $^6H_{15/2} \rightarrow {}^4G_{11/2}$ + $^4M_{21/2}$,$^6F_{1/2}$ (vis), and $^6F_{11/2}$ NIR region exhibit greater intensity than other transitions.

In the visible–NIR region, several weaker Dy^{3+} absorption features accompany the dominant bands. A shoulder between 570 and 600 nm is assigned to the $^6H_{15/2} \rightarrow {}^4G_{9/2}$ transition, with possible contribution from nearby $^4I_{11/2}$. In the 760–795 nm range, the spectral structure results from overlapping $^6H_{15/2} \rightarrow {}^6F_{3/2}$ (≈760–780 nm) and $^6H_{15/2} \rightarrow {}^6F_{5/2}$ (≈790–800 nm) transitions, whose Stark components are partially resolved in the glass host. Additional weak bands observed between 1400 and 1600 nm are attributed to higher Stark levels within the $^6F_{9/2}$–$^6H_{7/2}$ group, and their evolution with Dy^{3+} content reflects changes in the local crystal field rather than any sample-mixing artifact.

The slight variation in the absorption profile observed at different Dy^{3+} concentrations is attributed to concentration-induced modifications in the local field environment and Stark splitting effects within the glass network. These systematic spectral changes correlate well with the trends observed in density, refractive index, Judd–Ofelt parameters, and lifetime measurements, confirming that the variations arise from structural effects rather than any sample misidentification.



(**a**)



(**b**)

Figure 5. (**a**,**b**) Optical absorption spectra of Dy^{3+} ions doped PbO-B_2O_3-P_2O_5-ZnO-BaO glasses in the visible and NIR regions.

The decrease in peak intensities of absorption spectra, with increasing Dy^{3+} ion content more than 1.0 mol% in PbO-B_2O_3-P_2O_5-ZnO-BaO glasses, can be attributed to concentration quenching effects. At lower Dy^{3+} concentrations (1.0 mol%), the ions are uniformly distributed within the glass network, enabling effective optical absorption, whereas higher concentrations (1.5 and 2.0 mol%) promote stronger Dy^{3+}–Dy^{3+} interactions that facilitate non-radiative energy transfer through cross-relaxation and energy migration processes, leading to reduced absorption intensity and total optical conversion efficiency.

The optical energy gap (E_0) is a key parameter for understanding the electronic structure and optical response of glass materials. In this study, E_0 values for Dy^{3+}-doped samples were determined from the UV–Visible absorption spectra using Tauc's method (Figure 6). The extracted band gap primarily corresponds to the fundamental absorption edge of the host glass matrix arising from charge-transfer transitions between oxygen ions and network-forming cations. The Dy^{3+}, 4f–4f transitions appear as weak and sharp bands superimposed on the broad absorption edge and, owing to their localized and parity-forbidden character, do not affect the linear region used for band gap extrapolation. Hence, the evaluated E_0 values mainly reflect changes in the glass network structure rather than direct contributions from Dy^{3+} electronic transitions. With Dy^{3+} incorporation up to 1.0 mol%, a slight decrease in E_0 is observed, which is attributed to the generation of additional non-bridging oxygens and increased structural disorder. The variation in E_0 values indicates compositional modification of the glass network and confirms the suitability of the material for photonic and luminescent device applications [22,23].

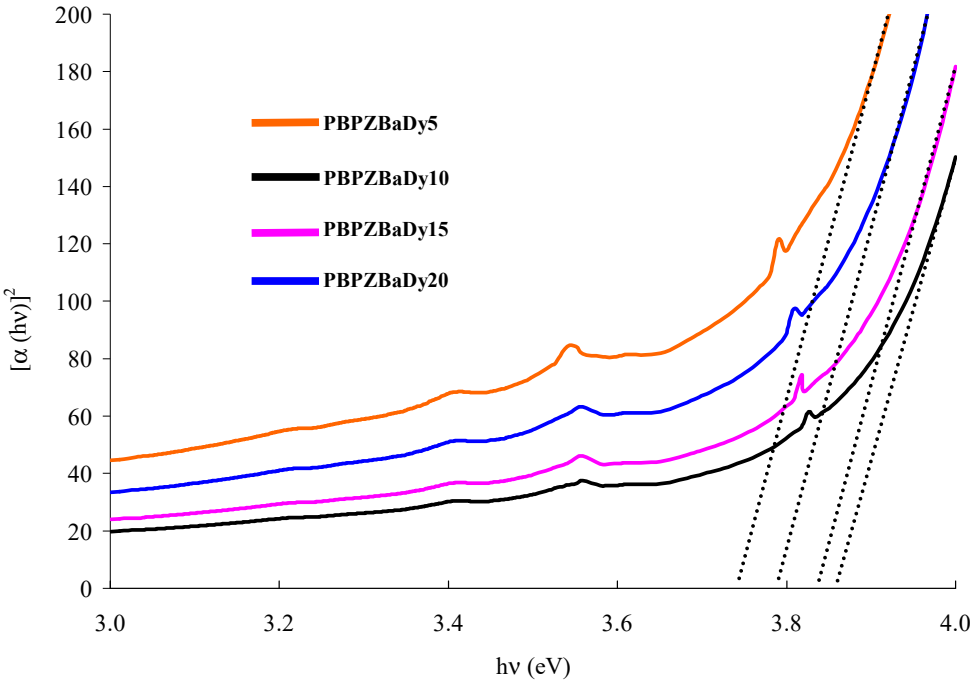


Figure 6. Tauc plots of Dy^{3+} ions doped PbO-B_2O_3-P_2O_5-ZnO-BaO glasses.

The absorption coefficient α is correlated with the optical band gap energy (E_o), which can be expressed using the following relation:

$$\alpha\ (h\nu) \propto B\ (h\nu - E_{opt})^{1/2} \quad (4)$$

Here, B corresponds to the band tailing parameter, while $h\nu$ represents the photonic energy. The value of E_0 was observed for 1.0 mol% of Dy^{3+}-doped glass composition (Table 1), suggesting an increased level of structural disorder within the glass network.

The experimental oscillator strengths (OS) (f_{exp}) corresponding to various absorption transitions of Dy^{3+} ions in PBPZBa glasses were evaluated from the absorption spectra using the standard equation [23].

$$f_{exp} = 4.319 \times 10^{-9} * \int \varepsilon(\nu) d\nu \quad (5)$$

The parameters involved in Equation (2) are defined in earlier reports [24–28].

The calculated electric dipole oscillator strengths (f_{cal}) for Dy^{3+} ions were obtained using Judd–Ofelt theory, as described in Equation (6), following the formulations reported in Refs. [24–28]. A close agreement between f_{exp} and f_{cal} values was observed, as evidenced by the root mean square deviation presented in Table 3.

$$f_{\mathrm{cal}} = \frac{8\pi^2 mc\nu\chi}{3h(2J+1)} \sum_{\lambda=2,4,6} \Omega_\lambda \left\langle f^N[\gamma, S, L]J \middle\| U^\lambda \middle\| f^N[\gamma', S', L']J' \right\rangle^2 \quad (6)$$

Table 3. The absorption band energies and the oscillator strengths (f $\times 10^{-6}$) for the transitions of Dy^{3+} ions in PbO-B_2O_3-P_2O_5-ZnO-BaO glasses.

Glass	PBPZBaDy5			PBPZBaDy10			PBPZBaDy15			PBPZBaDy20		
Transition $^6H_{15/2} \longrightarrow$	Barycenter (cm^{-1})	f_{exp} ($\times 10^{-6}$)	f_{cal} ($\times 10^{-6}$)	Barycenter (cm^{-1})	f_{exp} ($\times 10^{-6}$)	f_{cal} ($\times 10^{-6}$)	Barycenter (cm^{-1})	f_{exp} ($\times 10^{-6}$)	f_{cal} ($\times 10^{-6}$)	Barycenter (cm^{-1})	f_{exp} ($\times 10^{-6}$)	f_{cal} ($\times 10^{-6}$)
$^6H_{11/2}$	5988	0.051	0.056	5989	0.069	0.054	5990	0.052	0.051	5990	0.053	0.051
$^6F_{11/2}$	7812	0.232	0.216	7815	0.281	0.246	7817	0.241	0.257	7820	0.251	0.257
$^6F_{9/2}$	9095	0.164	0.118	9099	0.163	0.151	9102	0.161	0.167	9100	0.171	0.171
$^6F_{7/2}$	12,165	0.236	0.230	12,173	0.236	0.242	12,177	0.223	0.239	12,180	0.233	0.237
$^6F_{5/2}$	12,484	0.387	0.361	12,475	0.467	0.468	12,479	0.354	0.361	12,481	0.344	0.361
$^6F_{3/2}$	13,333	0.186	0.181	13,324	0.262	0.212	13,329	0.185	0.191	13,330	0.186	0.193
$^6F_{1/2}$	14,619	0.633	0.637	14,630	0.732	0.724	14,637	0.641	0.644	14,640	0.643	0.644
$^4F_{9/2}$	18,796	0.149	0.135	18,811	0.161	0.169	18,825	0.151	0.150	18,828	0.142	0.153
$^4I_{15/2}$	22,050	0.419	0.437	22,075	0.549	0.546	22,075	0.424	0.437	22,079	0.414	0.427
$^4G_{11/2}$	23,419	0.305	0.271	23,446	0.366	0.391	23,463	0.310	0.328	23,465	0.317	0.321
δ_{rms} ($\times 10^{-6}$)			±0.31			±0.46			±0.33			±0.30

Using Equation (6), the J-O parameters (Ω_2, $\Omega_{6,\text{ and }}$ Ω_4) were determined for all the Dy^{3+}-doped glass samples. The evaluated parameters follow the trend $\Omega_2 > \Omega_6 > \Omega_4$ (Table 3), which is consistent with earlier reports [29–31]. Among the studied samples, the glass $PBPZBaDy_{10}$ exhibited the lowest Ω_2 value, suggesting reduced asymmetry and lower covalency around Dy^{3+} ions. Notably, the Ω_2 value decreases progressively with Dy^{3+} ion concentration increased up to 1.0 mol%, beyond which an increase is observed for higher dopant levels (1.5 and 2.0 mol%).

This behavior indicates an initial reduction in the covalent character of the Dy-O bonds, followed by increased structural distortion at higher concentrations. The increase in Dy^{3+} content likely perturbs the glass network by enlarging the spacing between P–O–P and B–O–P linkages. Accordingly, the Dy–O bond lengths increase, leading to a weakened local crystal field around Dy^{3+} ions. This structural modification helps suppress phonon-assisted losses and cross-relaxation processes, thereby improving the optical performance of the glass system.

Figure 7 indicated emission spectra (λ_{exc} = 348 nm) for all the glass samples have their origin from excited level $^4F_{9/2}$ and exhibited the emission bands from $^4F_{9/2}$ to $^6H_{15/2}$ (blue ~ 484 nm), $^6H_{13/2}$ (yellow ~ 574 nm), and $^6H_{11/2}$ (red ~ 663 nm) correspondingly. Out of these, yellow emission (~574 nm) is usually most intense, leading to a white-light emission when balanced with blue emission. The emission intensity Y/B ratio values (for 0.5 mol% = 1.187, for 1.0 mol% = 1.185, for 1.5 mol% = 1.184, and for 2.0 mol% = 1.188) depend on factors such as Dy^{3+} content of the glass composition. The transition $^4F_{9/2} \rightarrow {}^6H_{13/2}$ ($\Delta L = 2$, $\Delta J = 2$) is observed to be hypersensitive. As the content of Dy_2O_3 increases, a significant enhancement in the intensity of the band ($^4F_{9/2} \rightarrow {}^6H_{13/2}$) is observed. However, beyond 1.0 mol%, the emission quenching occurs. Figure 8 illustrates the energy level diagram depicting different absorption and emission transitions associated with Dy^{3+} ions in the $PBPZBaDy_{10}$ glass sample.

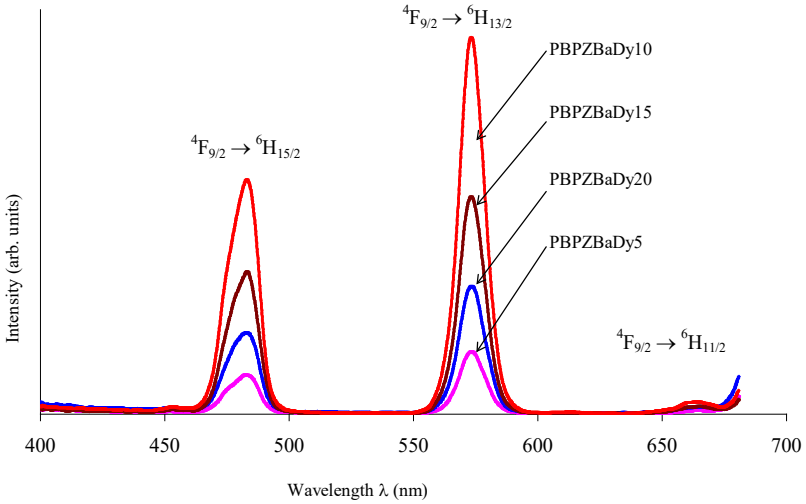


Figure 7. Emission spectra of Dy^{3+} ions doped PbO-B_2O_3-P_2O_5-ZnO-BaO glasses in the visible region.

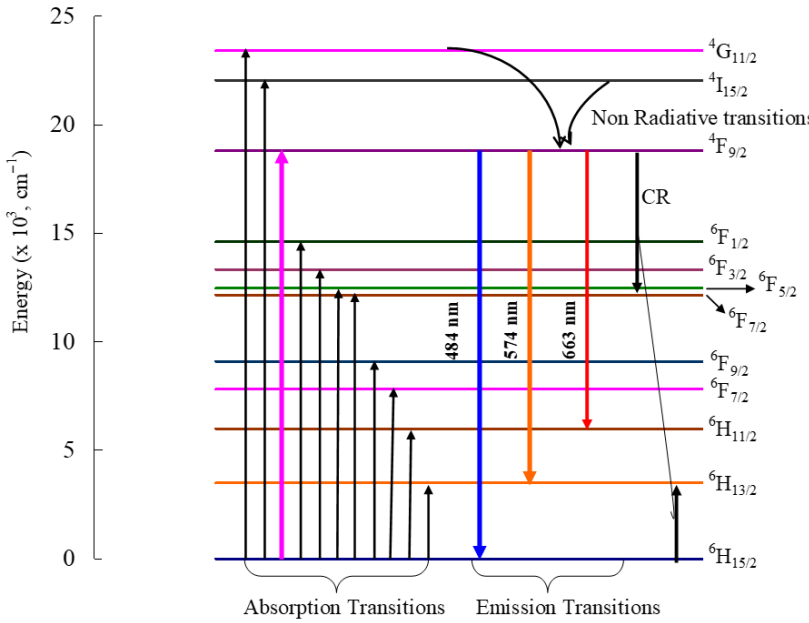


Figure 8. Energy level diagram representing different absorption and emission transitions of PBPZBaDy10 glass.

The emission transition probabilities associated with electric dipole transitions were evaluated using the relation:

$$A_{JJ'} = \frac{64\pi^4 e^2 v^3}{3h\,(2J+1)} \frac{n\,(n^2+2)^2}{9} \sum_{\lambda=2,4,6} \Omega_\lambda \left\langle f^N[\gamma, S,\ L]J \middle\| U^\lambda \middle\| f^N[\gamma', S', L']\,J' \right\rangle^2 \quad (7)$$

The detailed explanation of the above equation can be found in the referenced literature [7,25,28].

From the emission spectra, radiative parameters including the spontaneous emission probability (A), total radiative transition probability (A_T), radiative lifetime (τ), and fluorescence branching ratio (β) corresponding to the transitions originating from the $^4F_{9/2}$ excited state of Dy^{3+} ions were evaluated using conventional Equations (8)–(10) and were presented in Table 4 for PBPZBaDy10 glass.

$$\tau = \frac{1}{\sum_{J'} A_{JJ'}} \quad (8)$$

$$\beta_{JJ'} = \frac{A_{JJ'}}{\sum_{J'} A_{JJ'}} \quad (9)$$

$$\sigma(\lambda) = \frac{\lambda^4 A_{JJ'}}{8\pi c n^2 \Delta\lambda_{eff}} \quad (10)$$

Table 4. J-O parameters ($\Omega_\lambda \times 10^{-20}$, cm^{-2}) of Dy^{3+} ions doped in Pb_3O_4-B_2O_3-P_2O_5-ZnO-BaO glasses.

Glass Sample	**PBPZBaDy$_{10}$**			
Transition $^4F_{9/2} \downarrow$	Bary-center (cm^{-1})	A (s^{-1})	β (%)	σ_P^E ($\times 10^{-22}$, cm^2)
$\longrightarrow {}^6H_{15/2}$	20,655	229	12.12	0.913
$\longrightarrow {}^6H_{13/2}$	17,422	1547	81.89	2.642
$\longrightarrow {}^6H_{11/2}$	15,140	113	5.98	0.655
		A_T = 1889 s^{-1}		τ_{rad} = 0.529 ms

The details of the above equations (Equations (8)–(10)) were explained in Refs [28–30].

We have observed the radiative parameters for PBPZBaDy10 glass tabulated in Table 5, attributing the highest radiative values. This enhancement is attributed to the optimal distribution of Dy^{3+} ions at a doping concentration of 1.0 mol%, which promotes radiative transitions by effectively suppressing non-radiative losses. However, at higher Dy^{3+} contents (1.5 to 2.0 mol%), increased ion-ion interactions, cross-relaxation mechanisms, and energy transfer between adjacent Dy^{3+} ions result in concentration quenching effects. These processes diminish the radiative efficiency, leading to reduced fluorescence lifetimes and lower branching ratio values. Consequently, Dy^{3+} mixed 1.0 mol% is identified as optimal for achieving efficient luminescence with superior radiative properties in the present glass system.

Table 5. Various radiative properties of transitions of 1.0 mol% Dy^{3+} ions in PbO-B_2O_3-P_2O_5-ZnO-BaO glass.

Glass Sample	**Ω_2**	**Ω_4**	**Ω_6**	**Trend**
PBPZBaDy5	9.13	2.74	3.05	$\Omega_2 > \Omega_6 > \Omega_4$
PBPZBaDy10	4.62	0.97	2.15	$\Omega_2 > \Omega_6 > \Omega_4$
PBPZBaDY15	5.60	1.44	3.11	$\Omega_2 > \Omega_6 > \Omega_4$
PBPZBaDy20	6.35	2.76	3.74	$\Omega_2 > \Omega_6 > \Omega_4$
PbPKANDy10 [29]	11.74	2.64	2.86	$\Omega_2 > \Omega_6 > \Omega_4$
TWZDy10 [30]	6.910	0.990	1.010	$\Omega_2 > \Omega_6 > \Omega_4$
BLND [31]	11.99	3.92	3.94	$\Omega_2 > \Omega_6 > \Omega_4$

Figure 9 shows the decay profile of PBPZBaDy10 glass from the $^4F_{9/2}$ level; corresponding lifetime values are listed in Table 6. A comparatively longer radiative lifetime is observed in the glass doped with 1.0 mol%, suggesting a more covalent bonding environment around the Dy^{3+} ions, along with higher vibrational frequencies. The glass PBPZBaDy10 exhibits the highest quantum efficiency (η = 91.68), which enhances the yellow–blue (Y/B) luminescence, bringing it closer to the white-light region compared to other glasses.

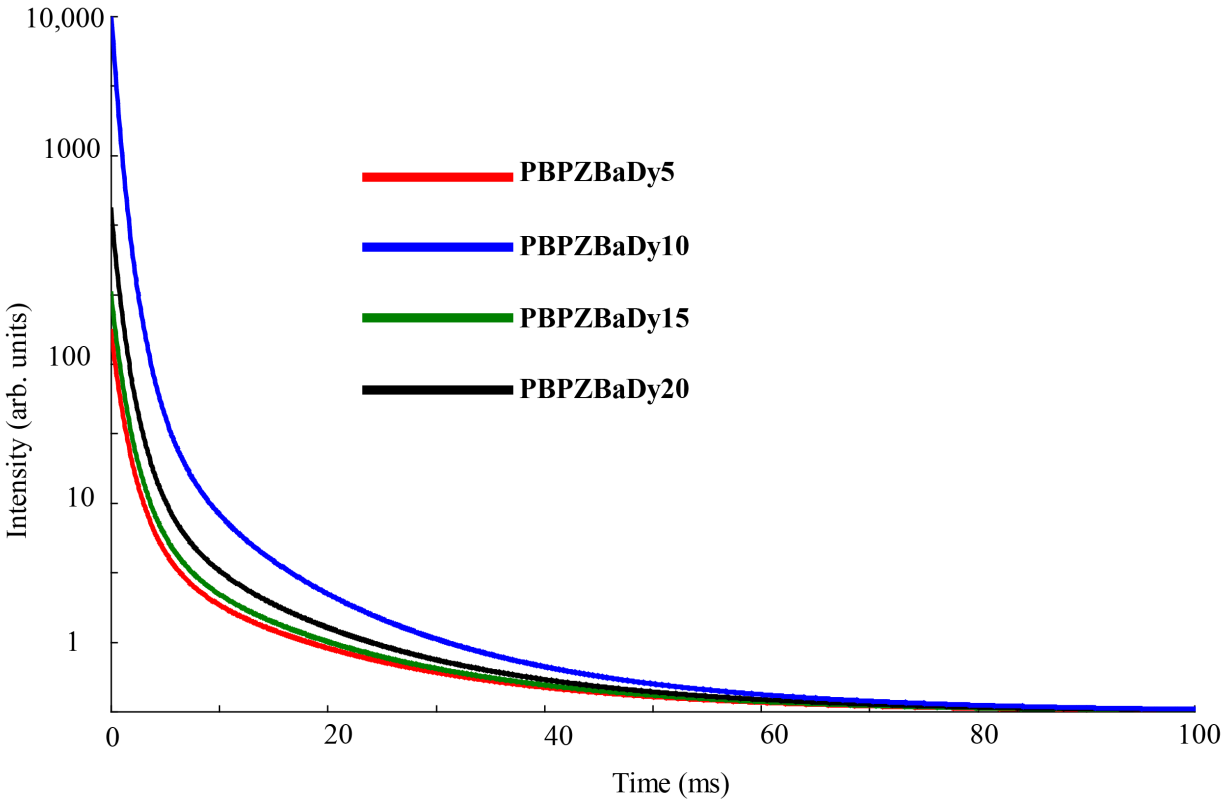


Figure 9. Fluorescence decay curves for PbO-B_2O_3-P_2O_5-ZnO-BaO glass.

Table 6. The experimental (τ_{exp}, μs) and calculated (τ_R, μs) life times and quantum efficiency (η, %) of Dy^{3+} ions doped in PbO-B_2O_3-P_2O_5-ZnO-BaO glasses.

Glass Sample	Measured (τ_{exp} μs)	Calculated (τ_R, μs)	Quantum Efficiency (η%)
PBPZBaDy5	361	437	82.61
PBPZBaDy10	485	529	91.68
PBPZBaDy15	438	496	88.30
PBPZBaDy20	382	441	86.66

The obtained quantum efficiency is comparable to or slightly higher than many previously reported Dy^{3+}-doped phosphate, borate, and tellurite glasses, where efficiencies typically fall in the range of ~75–90%, depending on host matrix and dopant concentration. This confirms that the present PbO–B_2O_3–P_2O_5–ZnO–BaO glass system provides an efficient radiative environment for Dy3+ ion emission.

Figure 10 shows that chromaticity coordinates (x = 0.33, y = 0.41) lie in proximity to the white-light region of the CIE 1931 chromaticity diagram. As the Dy^{3+} ion concentration increases beyond 1.0 mol%, a gradual shift in the emission color toward the yellowish region is observed. Therefore, the 1.0 mol% Dy^{3+} composition provides an optimal balance between blue and yellow emissions, resulting in high quantum efficiency and chromaticity coordinates close to the ideal white-light region, comparable to other similar Dy^{3+}-doped glass systems reported in the literature [7,29–31].

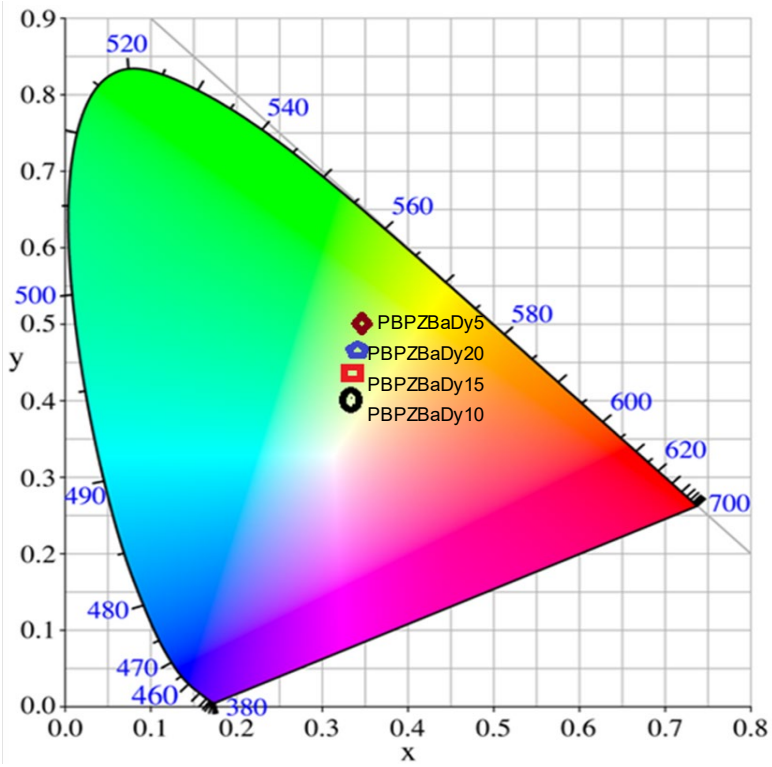


Figure 10. CIE plot represents color coordinate corresponding white emission of Dy^{3+} ions doped PbO-B_2O_3-P_2O_5-ZnO-BaO glasses.

4. Conclusions

The present investigation demonstrates that Dy^{3+} ions doped PbO-B_2O_3-P_2O_5-ZnO-BaO glasses exhibited the remarkable luminescent behavior, with the sample containing 1.0 mol% Dy_2O_3 (PBPZBaDy10) showing superior optical performance. This composition achieved the highest luminescence intensity, radiative transition probabilities, and quantum efficiency (η = 91.68%). The emission spectra revealed two strong bands corresponding to the $^4F_{9/2} \rightarrow {}^6H_{15/2}$ (blue) and $^4F_{9/2} \rightarrow {}^6H_{13/2}$ (yellow) transitions, whose balanced intensities produced near-white light with chromaticity coordinates (x = 0.33, y = 0.41) in the CIE 1931 color space. Judd–Ofelt analysis exhibited the parameter trend $\Omega_2 > \Omega_6 > \Omega_4$, indicating an asymmetric and moderately covalent environment around Dy^{3+} ions. Concentration quenching beyond 1.0 mol% was primarily due to Dy^{3+}–Dy^{3+} cross-relaxation and non-radiative energy transfer processes. The novelty of this work lies in developing a multicomponent Pb–B–P–Zn–Ba glass matrix that simultaneously provides high optical transparency, chemical stability, and efficient single-ion white-light emission without co-dopants. These findings establish the glass PBPZBaDy10 as a promising material for next-generation white-light-emitting diodes (WLEDs), optical sensors, and photonic device applications.

Author Contributions: V.R.K.: Conceptualization, Investigation, Data curation, Writing original draft; S.V.B.S.: Methodology; K.K.K.: Data curation; B.V.M.: Formal analysis; K.S.: Investigation; L.M.: Editing; M.N.: Investigation; V.S.: Formal analysis; L.V.: Methodology, Data curation, Writing original draft, Editing; J.L.: Supervision. All authors have read and agreed to the published version of the manuscript.

Funding: This research received no external funding.

Data Availability Statement: The data presented in this study are available on request from the corresponding author. The data are not publicly available due to laboratory data management policies and the large size of the raw experimental datasets.

Conflicts of Interest: The authors declare no conflict of interest.

References

1. Chandrappa, V.; Basavapoornima, C.; Venkatramu, V.; Depuru, S.R.; Kaewkhao, J.; Pecharapa, W.; Jayasankar, C.K. A critical review and future prospects of Dy^{3+}-doped glasses for white light emission applications. *Optik* **2022**, *266*, 169583. [CrossRef]
2. Li, Y.; Xu, S.; Chen, J.; Zhang, X.; Liu, H.; Chi, Y.; Sun, X.; Mahadevan, C.K. Structural and luminescence properties of Dy^{3+}activated niobiosilicate glass with high thermal stability for W-LED application. *Ceram. Int.* **2024**, *50*, 14571–14580. [CrossRef]
3. ReddiBabu, M.; Rao, N.M.; Babu, A.M.; Jaidass, N.; Moorthy, C.K.; Moorthy, L.R. Effect of Dy^{3+}ions concentration on optical properties of lead borosilicate glasses for white light emission. *Optik* **2016**, *127*, 3121–3126. [CrossRef]
4. Maheshwari, K.; Rao, A.S. Photoluminescence downshifting studies of thermally stable Dy^{3+}ions doped phosphate glasses for photonic device applications. *Opt. Mater.* **2022**, *129*, 112518. [CrossRef]
5. Indhrapriyadarshini, A.; Naseer, K.A.; KomalPoojha, M.K.; Marimuthu, K.; Sayyed, M.I.; Alqahtani, M.S. Significance of multicomponent modifiers incited Dy^{3+}ions doped boro-phosphate glasses for radiation shielding applications. *Optik* **2024**, *304*, 171755. [CrossRef]
6. Poria, K.; Lohan, R.; Bhatia, S.; Kumar, A.; Singh, R.; Deopa, N.; Punia, R.; Shahi, J.S.; Rao, A.S. Lumino-structural properties of Dy^{3+}activated Na3Ba2LaNb10O30phosphors with enhanced internal quantum yield for w-LEDs. *RSC Adv.* **2023**, *13*, 11557–11568. [CrossRef] [PubMed]
7. Khondara, S.; Yasaka, P.; Boonin, K.; Intachai, N.; Kim, H.J.; Kaewkhao, J. White light emission from Dy^{3+}ion doped boro-tellurite glass potential for optical and thermoluminescence material applications. *Radiat. Phy. Chem.* **2025**, *237*, 113007. [CrossRef]
8. Krishnamacharyulu, N.; Mohini, G.J.; Baskaran, G.S.; Kumar, V.R.; Veeraiah, N. Effect of ZrO_2 on the bioactive properties of B_2O_3–SiO_2–P_2O_5–Na_2O–CaO glasssystem. *J. Non-Cryst. Solids* **2016**, *452*, 23–29. [CrossRef]
9. Kumari, C.V.; Sobhanachalam, P.; Jayasankar, C.K.; Veeraiah, N.; Kumar, V.R. Bioactive properties of CuO doped CaF_2-CaO-B_2O_3-P_2O_5-MO (M = Ba, Sr, Zn, Mg) glasses. *Ceram. Int.* **2017**, *43*, 4335–4343. [CrossRef]
10. Satyanarayana, T.; Kityk, I.V.; Brik, M.G.; Kumar, V.R.; Veeraiah, N. Fluorescence features of Tm^{3+} ions in PbO–Sb_2O_3–B_2O_3 glass ceramics. *Phys. B* **2010**, *405*, 1872–1880. [CrossRef]
11. Gandhi, Y.; Rajanikanth, P.; SundaraRao, M.; Kumar, V.R.; Veeraiah, N.; Piasecki, M. Effect of tin ions on enhancing the intensity of narrow luminescence line at311 nm of Gd^{3+} ions in Li_2O–PbO–P_2O_5 glass system. *Opt. Mater.* **2016**, *57*, 39–44. [CrossRef]
12. Kumar, V.R.; Giridhar, G.; Jayasankar, C.K.; Veeraiah, N. The energy transfer efficiency from Yb^{3+} to Nd^{3+} in SrO–Pb_3O_4–ZnO–P_2O_5 glasssystem-Influence of lead ions. *J. Lumin.* **2017**, *187*, 281–289. [CrossRef]
13. Rama Chandra Rao, M.V.; Hariprasad, D.; Jyothi, B.; Kumar, D.P.; Naresh, P.; Lakshmi, G.V.; Nagarjuna, M.; Kumar, V.R.; Gandhi, Y.; Veeraiah, N. Luminescence properties of Ho^{3+} ions in Pb_3O_4-B_2O_3-P_2O_5-ZnO-AIIIx (AIIIx = Al_2O_3, Ga_2O_3, and In_2O_3) glasses. *Optik* **2025**, *328*, 172315. [CrossRef]
14. Gandhi, Y.; Kityk, I.V.; Brik, M.G.; Rao, P.R.; Veeraiah, N. Role of tungsten coordination and valence states in ZnF_2-WO_3-TeO_2 glasses on the emissionfeatures of Nd^{3+}, Sm^{3+} and Eu^{3+} ions in the visible and IR spectral ranges. *J. Alloys Compd.* **2010**, *508*, 278–291. [CrossRef]
15. Kumar, V.R.; Giridhar, G.; Veeraiah, N. Influence of modifier oxide on emission features of Dy^{3+} ion in Pb_3O_4-ZnO-P_2O_5 glasses. *Opt. Mater.* **2016**, *60*, 594–600. [CrossRef]
16. Rao, K.J. Structural Chemistry of Glasses. *J. Am. Chem. Soc.* **2003**, *125*, 7479–7480. [CrossRef]
17. Sudhakar, K.S.V.; Reddy, M.S.; SrinivasaRao, L.; Veeraiah, N. Influence of modifier oxide on spectroscopic and thermoluminescence characteristics of Sm^{3+} ion in antimony borate glass system. *J. Lumin.* **2008**, *128*, 1791–1798. [CrossRef]
18. Karunakaran, R.T.; Marimuthu, K.; Babu, S.S.; Arumugam, S. Dysprosium doped alkali fluoroborate glasses-Thermal, structural and optical investigations. *J. Lumin.* **2010**, *130*, 1067–1072. [CrossRef]
19. Kalpana, T.; Brik, M.G.; Sudarsan, V.; Naresh, P.; Kumar, V.R.; Kityk, I.V.; Veeraiah, N. Influence of Al^{3+} ions on luminescence efficiency of Eu^{3+} ions in barium boro-phosphate glasses. *J. Non-Cryst. Solids* **2015**, *419*, 75–81. [CrossRef]
20. Ali, A.A. Optical properties of Sm^{3+}-doped CaF_2 bismuth borate glasses. *J. Lumin.* **2009**, *129*, 1314. [CrossRef]
21. Schubert, E.F. *Light Emitting Diodes*, 2nd ed.; Cambridge University Press: Cambridge, UK, 2006.
22. Luo, M.; Chen, B.; Li, X.; Zhang, J.; Xu, S.; Zhang, X.; Cao, Y.; Sun, J.; Zhang, Y.; Wang, X.; et al. Fluorescence decay route of optical transition calculation for trivalent rare earth ions and its application for Er^{3+}-doped $NaYF_4$ phosphor. *Phys. Chem. Chem. Phys.* **2020**, *22*, 25177–25183. [CrossRef]
23. Ram, G.C.; Narendrudu, T.; Suresh, S.; Kumar, A.S.; Rao, M.S.; Kumar, V.R.; Rao, D.K. Investigation of luminescence and laser transition of Dy^{3+} ion in P_2O_5-PbO-Bi_2O_3-R_2O_3 (R ¼ Al, Ga, In) glasses. *Opt. Mater.* **2017**, *66*, 189–196. [CrossRef]
24. Kumar, V.R.; Giridhar, G.; Veeraiah, N. Concentration dependence of luminescence efficiency of Dy^{3+} ions in strontium zinc phosphate glasses mixed with Pb_3O_4. *Luminescence* **2017**, *32*, 71–77. [CrossRef]
25. Judd, B.R. Optical absorption intensities of rare-earth ions. *Phys. Rev.* **1962**, *127*, 750–761. [CrossRef]
26. Ofelt, G.S. Intensities of crystal spectra of rare-earth ions. *J. Chem. Phys.* **1962**, *37*, 511–520. [CrossRef]

27. Linganna, K.; Rao, C.S.; Jayasankar, C.K. Optical properties and generation of white light in Dy^{3+} doped lead phosphate glasses. *J. Quant. Spectrosc. Radiat. Transf.* **2013**, *118*, 40–48. [CrossRef]
28. Venkataiah, G.; Jayasankar, C.K. Dy^{3+}-doped tellurite-based tungsten-zirconium glasses: Spectroscopic study. *J. Mol. Struct.* **2015**, *1084*, 182–189. [CrossRef]
29. Yen, W.M.; Shionoya, S. *Phosphor Handbook*; CRC Press: New York, NY, USA, 1999.
30. Billmeyer, F.W.; Saltzman, M., Jr. *Principles of Colour Technology*; Wiley: New York, NY, USA, 1981.
31. Reddy, M.C.S.; Rao, B.A.; Brik, M.G.; Reddy, A.P.; Rao, P.R.; Jayasankar, C.K.; Veeraiah, N. Emission characteristics of Dy^{3+} ions in lead antimony borate glasses. *Appl. Phy. B–Lasers Optics* **2012**, *108*, 455–461. [CrossRef]

Disclaimer/Publisher's Note: The statements, opinions and data contained in all publications are solely those of the individual author(s) and contributor(s) and not of MDPI and/or the editor(s). MDPI and/or the editor(s) disclaim responsibility for any injury to people or property resulting from any ideas, methods, instructions or products referred to in the content.